CD22 Antigen Is Broadly Expressed on Lung Cancer Cells and Is a Target for Antibody-Based Therapy

Joseph M. Tuscano[1,2], Jason Kato[1], David Pearson[3], Chengyi Xiong[1], Laura Newell[4], Yunpeng Ma[1], David R. Gandara[1], and Robert T. O'Donnell[1,2]

Abstract

Most patients with lung cancer still die from their disease, necessitating additional options to improve treatment. Here, we provide evidence for targeting CD22, a cell adhesion protein known to influence B-cell survival that we found is also widely expressed in lung cancer cells. In characterizing the antitumor activity of an established anti-CD22 monoclonal antibody (mAb), HB22.7, we showed CD22 expression by multiple approaches in various lung cancer subtypes, including 7 of 8 cell lines and a panel of primary patient specimens. HB22.7 displayed *in vitro* and *in vivo* cytotoxicity against CD22-positive human lung cancer cells and tumor xenografts. In a model of metastatic lung cancer, HB22.7 inhibited the development of pulmonary metastasis and extended overall survival. The finding that CD22 is expressed on lung cancer cells is significant in revealing a heretofore unknown mechanism of tumorigenesis and metastasis. Our work suggests that anti-CD22 mAbs may be useful for targeted therapy of lung cancer, a malignancy that has few tumor-specific targets. *Cancer Res; 72(21); 5556–65. ©2012 AACR.*

Introduction

In the United States, lung cancer is the most common cause of cancer-related death in men and women (1). Despite refinements in platinum-based chemotherapy and several newly approved targeted agents, the median overall survival of patients with advanced, unresectable, non–small cell lung cancer (NSCLC) is only 9 to 12 months (2, 3). Monoclonal antibodies (mAb) and tyrosine kinase inhibitors that inhibit signaling from EGF receptor (EGFR) and VEGF provide clinical benefit to some patients with NSCLC. Still, the EGFR inhibitor, erlotinib, is most effective only in the small subset of patients with activating mutations in EGFR, and even these most sensitive neoplasms inevitably develop resistance. Similarly, the VEGF-targeted mAb, bevacizumab, adds only incrementally to progression-free and overall survival (4–6). New therapeutic approaches are essential to advance the treatment of lung cancer. We recently identified CD22 as a potential new target. Herein, we characterize the expression of CD22 in lung cancer and report that an anti-CD22 mAb developed for the treatment of non-Hodgkin lymphoma (NHL), HB22.7, effectively binds lung cancer cells and mediates specific *in vitro* and *in vivo* killing.

CD22 is a 140 kDa transmembrane sialo-adhesion protein expressed by nearly all mature B cells and NHL (7–10). CD22 is a member of the immunoglobulin (Ig) superfamily and has seven extracellular Ig-like domains. The 2 amino-terminal Ig domains of CD22 mediate cell adhesion to widely distributed α (2, 6) sialic-acid–bearing ligands and B-cell homing to endothelial cells (7). An important function of CD22 in B cells is to modulate B-cell antigen receptor (BCR) signaling. Within the cytoplasmic tail of CD22 are immunoreceptor tyrosine activation motifs (ITAM) and tyrosine inhibitory motifs (ITIM; refs. 11, 12). CD22 ITAMs become phosphorylated upon BCR activation by src-like kinases, enhancing the recruitment of protein tyrosine phosphatases to CD22. Because of the close proximity of the BCR, these CD22-associated phosphatases then dephosphorylate BCR components resulting in attenuation of BCR signaling. The consequences of BCR-independent engagement of CD22 on B-cell function as well as the downstream signal transduction events triggered through CD22 have recently been explored. We and others have shown that potent and direct activation of CD22 by ligand binding and cross-linking is cytotoxic for some B-cell NHL (11–15).

It has heretofore been thought that CD22 was exclusively expressed on B cells. Our observation that CD22 is expressed on lung cancer cells may ultimately lead to the identification of a novel and specific target for antibody-mediated therapy for lung cancer, which has few tumor-specific targets. We have shown that HB22.7 has significant anti-NHL preclinical efficacy and, as with many mAb-based therapies, little toxicity (16). Therefore, further exploration of the CD22-HB22.7 interaction in lung cancer and successful development of HB22.7

Authors' Affiliations: [1]Division of Hematology and Oncology, Department of Internal Medicine, University of California Davis Comprehensive Cancer Center, Sacramento; [2]Department of Veteran's Affairs, Northern California Healthcare System, Mather; [3]California Northstate University College of Pharmacy, Rancho Cordova, California; and[4]Oregon Health and Science University, Portland, Oregon

Corresponding Author: Joseph Tuscano, Department of Internal Medicine, Division of Hematology and Oncology, University of California Davis Comprehensive Cancer Center, 4501 X Street, Suite 3016, Sacramento, CA 95817. Phone: 916-734-3771; Fax: 916-734-2361; E-mail: joseph.tuscano@ucdmc.ucdavis.edu.

doi: 10.1158/0008-5472.CAN-12-0173

could result in a useful new therapy for patients with lung cancer.

Materials and Methods

Chemicals

Goat anti-mouse IgG fluorescein, goat anti-mouse IgG PE-Cy5, and rabbit anti-human CD22 (H-221) were purchased from Santa Cruz Biotechnology. Anti-mouse HRP antibody was purchased from Dako. The anti-CD22 antibody used for immunohistochemistry, NCL-CD22-2, was purchased from Leica Microsystems. Rituximab was obtained from the UC Davis Cancer Center Pharmacy (Sacramento, CA). The anti-CD22 mAb, HB22.7, was purified from ascites and has been previously characterized (9). MTS was purchased from Promega. All other chemicals were purchased from Sigma-Aldrich.

Cell lines

The CD22-positive human Burkitt lymphoma cell lines, Ramos and Raji, as well as the lung cancer cell lines: A549, H1355, H1975, Calu-1, H1650, and H727 were purchased from American Type Culture Collection. The lung cancer cell lines HCC827 and A427 were a gift from Dr. Phil Mack (Davis Department of Internal Medicine, University of California, Sacramento, CA). Cells were grown in RPMI-1640 (NHL cell lines) or Dulbecco's Modified Eagle's Medium (lung cancer cell lines) supplemented with 10% FBS, 50 U/mL penicillin G, and 50 μg/mL streptomycin sulfate. Cells were maintained at 37°C in 5% CO_2 and 90% humidity. After 2 passages, vials were frozen and stored in liquid nitrogen for future use. Fresh vials of cells were periodically thawed and used for *in vitro* experiments to ensure that changes to cells did not occur over time/passages in culture. For xenograft studies, a fresh vial of cells was thawed 7 to 10 days before tumor cell implantation.

Flow cytometry

Flow cytometry was used to assess CD22 surface expression and HB22.7 binding. HB22.7 (25 μg/mL) was incubated with cells for 30 minutes on ice followed by 3 washes with ice-cold fluorescence-activated cell sorting (FACS) buffer [phosphate buffered saline (PBS) + 4% FBS]. Goat anti-mouse IgG-fluorescein isothiocynate (FITC; 1:50 dilution) was added to cells and incubated on ice for 30 minutes followed by 3 washes with FACS buffer. Ten thousand events were analyzed using a Becton-Dickinson FACSCalibur cytometer.

Real-time PCR

Real-time PCR (RT-PCR) was conducted as previously described (15). Briefly, total RNA was extracted from cells using the RNeasy Mini Kit (Qiagen) following the manufacturer's protocol. cDNA was synthesized from 1 μg of total RNA using the SuperScript III First-Strand Synthesis System for RT-PCR (Invitrogen). PCR conditions, including CD22 primer selection, concentration, and annealing temperature, were previously optimized. CD22 primer sequences were: 5′-GGTCAGCCTCCAATGTGACT-3′ (forward) and 5′-CTGGCTCTGTGTCCTCTTCC-3′ (reverse). GAPDH was used as a reference gene.

Western blot analysis

CD22 immunoblotting was conducted as previously described with slight modifications (14, 15). A plasma membrane protein extraction kit (BioVision) was used to enhance detection of CD22. A plasma membrane protein and cytosol preparation were run on 10% SDS-PAGE, followed by transfer to a nitrocellulose membrane. Membranes were blocked with 5% bovine serum albumin (BSA) in TBS-T, rinsed, then incubated at 4°C overnight in primary antibody (anti-CD22) diluted 1:1,000 in 5% BSA in TBS-T. Washed membranes were incubated for 1 hour at room temperature with anti-rabbit HRP conjugate diluted 1:10,000 in 5% BSA in TBS-T. Membranes were washed then probed with ECL Advanced Detection Kit (GE Life Sciences). Because of difficulty in quantifying total protein from the plasma membrane protein and cytosol preparations, the loading from the various cell lines may not be equal. The goal of this experiment was not to make a quantitative comparison but rather to verify expression of CD22 at the protein level.

Northern blot analysis

CD22 Northern blot analysis was conducted as described (17). Briefly, total RNA was size separated via agarose-formaldehyde PAGE and transferred to a nylon membrane. CD22-specific RNA was detected with a DIG-dUTP–labeled DNA probe generated using CD22-specific PCR primers following the manufacturer's recommendations (Roche).

CD22 siRNA transfection and real-time quantitative PCR

The NHL cell line Raji and the lung cancer cell lines A549 and H727 were transfected with CD22 siRNA (Santa Cruz Biotechnology) using Lipofectamine 2000 (Invitrogen) according to the manufacturer's instructions. Total RNA was extracted from the cells 48 hours after transfection using TRIzol reagent (Invitrogen). cDNA was synthesized as described above. Real-time quantitative PCR was conducted using the SYBR GreenER qPCR SuperMix (Invitrogen) and an iQ5 Real-Time PCR detection system (Bio-Rad) for CD22 (Genbank accession no. NM_001771) and β-actin (Genbank accession no. NM_001101). The sequences of primers for CD22 amplification were: 5′- GACTGAGAAATGGATGGAACG-3′ (forward) and 5′-CATAGCAGGAGAAATTCAGCA-3′ (reverse), the primers for β-actin were 5′-GAGCGCGGCTACAGCTT-3′ (forward) and 5′-TCCTTAATGTCACGCACGATTT-3′ (reverse). PCR conditions, including primer concentration and annealing temperature were optimized for each amplicon. A melt curve was included following all PCR reactions to ensure minimal amount of artifact formation. A standard curve was generated for each target-specific amplicon using six 5-fold dilutions of cDNA and the efficiency of each RT-PCR reaction was determined. β-actin was used as a reference gene for all assays. The software package Q-Gene (18, 19) was used to determine the mean normalized expression for each gene.

Immunohistochemistry

Five- to seven-micrometer paraffin-embedded primary lung cancer and tonsil sections were prepared using a high temperature antigen retrieval method. Briefly, deparaffinized sections were incubated in epitope retrieval solution (0.01 mol/L citrate buffer, pH 6.0) at 100°C in a pressure cooker for 1 minute. Slides were washed with TBS and blocked with diluted (1:50) normal serum, then immunostained with a mAb against CD22 at 1:40 (NCL-CD22-2, Leica Microsystems) for 6 hours. After washing with TBS, the slides were incubated with a biotinylated anti-mouse secondary antibody (Dako), washed with TBS, and incubated with streptavidin-HRP (Envision Flex Kit, Dako). Bound antibody was revealed by adding the substrate 3,3-diaminobenzidine. Sections were counterstained with hematoxylin and eosin.

In vitro cytotoxicity

Cells (2×10^4 per sample) were plated in triplicate in 96-well plates in a volume of 100 μL. Cells were treated with HB22.7 or rituximab at a concentration of 50 μg/mL. Untreated control cells received media only. After a 72-hour incubation, cell viability was assessed using the CellTiter 96 AQueous One Solution Cell Proliferation Assay (Promega) according to the manufacturer's instructions. Cell viability as a percent of the untreated control was calculated as follows: [(OD490 treated−OD490 background)/(OD490 control−OD490 background)×100]. The mean ± SD of 3 separate experiments conducted in triplicate is shown.

Internalization assay

Internalization of CD22 was assessed using previously described methods. The first method correlates the cytotoxicity of an antibody–saporin conjugate to the internalization of the target antigen (20, 21). Reagents were purchased from Advanced Targeting Systems and conducted according to the manufacturer's instructions. Briefly, 1.5×10^3 A549 and H1650 cells were seeded in 96-well plates in 90 μL media and allowed to adhere overnight. Serial dilutions of mouse HB22.7 were incubated with 10 μg/mL of saporin-conjugated goat anti-mouse IgG (Mab-ZAP) for 15 minutes at room temperature. The HB22.7–Mab–ZAP conjugate (10 μL) was added to each well yielding a final concentration of 1 μg/mL Mab-ZAP. Saporin-conjugated goat IgG (goat IgG-SAP) was used as a nontargeted control for Mab-ZAP. After a 72-hour incubation, cell viability was assessed by MTS assay.

The second method used a flow cytometry approach to assess CD22 internalization (21). Cells were incubated with HB22.7 (25 μg/mL) for 30 minutes on ice followed by 3 washes with ice-cold FACS buffer and resuspended in growth medium. Cells were then kept at 4°C or transferred to 37°C and incubated for 90 minutes. To detect surface-bound HB22.7, cells were incubated with a 1:50 dilution of goat anti-mouse IgG-PE-Cy5 for 30 minutes on ice. Cells were washed 3 times and 10,000 events were analyzed as mentioned previously. As a control, cells were also untreated or treated with goat anti-mouse IgG-PE-Cy5 alone.

ADCC/CDC assay

Peripheral blood mononuclear cells (PBMC) were isolated from whole blood collected into citrated vacuum tubes from healthy volunteers using standard protocol. Following isolation, PBMCs were placed in media and activated using human IL-2 (Chiron) at 1,000 U/mL overnight at 37°C. For the CDC assay, human serum complement (Quidel) was added at a 1:10 dilution. Activated PBMCs or human serum complement were incubated with A549 cells in the presence and absence of humanized HB22.7 (50 μg/mL). The activated PBMCs were added at 10 times the number of target cancer cells with the appropriate controls. The cells were incubated for 48 hours and cytotoxicity was assessed using the CytoTox 96 Non-Radioactive Cytotoxicity Assay (Promega) following the manufacturer's instructions.

I-PET

Copper-64 (^{64}Cu)-labeled HB22.7 was used to determine the ability of HB22.7 to specifically target A549 cells *in vivo* as previously described (22). ^{64}Cu was produced on the biomedical cyclotron at Washington University (Seattle, WA) and supplied as $^{64}CuCl_2$ (0.1 mol/L HCl). The bifunctional chelating agent, DOTA (1, 4, 7, 10-tetraazacyclododecane N, N′, N″, N‴-tetraacetic acid (DOTA) contains a reactive functionality to form a covalent attachment to proteins and a strong metal-binding group to chelate radiometals. DOTA-HB22.7 was prepared by incubation with DOTA-NHS-ester at pH 5.5. DOTA-HB22.7 was labeled with ^{64}Cu-acetate in 0.1 mol/L ammonium acetate, pH 5.5. After incubation, 1 mmol/L EDTA terminated the reaction. High-performance liquid chromatography (HPLC) purification was then conducted to purify the ^{64}Cu-DOTA-HB22.7.

Xenograft studies

Female, 6- to 8-week old Balb/c nude mice were obtained from Harlan Sprague Dawley and maintained in microisolation cages under pathogen-free conditions in the UC Davis animal facility. All procedures were conducted under an approved protocol according to guidelines specified by the National Institute of Health Guide for Animal Use and Care. Three days after whole body irradiation (400 rads), 5×10^6 A549, PC-3, or H1650 cells were implanted subcutaneously on the flank. Either 24 hours after tumor cell implantation (preemptive) or when tumor volumes reached 100 mm^3, mice were randomly divided into treatment groups ($n = 8$–10/group) and treated weekly for 4 weeks. All treatments were administered through the tail vein. Tumors were measured twice per week using digital calipers and tumor volumes were calculated using the equation: (length × width × depth) × 0.52. Mice were euthanized when the tumor reached 15 mm in any dimension, if they became moribund, or at the end of the 84-day study.

The metastatic xenograft model has been previously described (17, 23). Briefly, 1×10^6 A549 cells were resuspended in 100 μL media and injected into the tail vein. Treatment with HB22.7 or an IgG isotype-matched control was initiated 24 hours after tumor cell implantation and mice were treated weekly for 4 weeks. Mice were euthanized when they became moribund (although the majority of mice from the control

group died by day 14) and lungs were harvested and examined histologically. To facilitate comparison of the development of lung metastasis, HB22.7-treated mice were also euthanized at day 14. However, to facilitate a comparison of overall survival, a cohort of 5 HB22.7-treated mice were not euthanized but monitored for an additional 62 days.

Statistical analysis

In vitro cytotoxicity data was analyzed by a 2-tailed, unpaired Student *t* test. Tumor volume data were analyzed using Kaplan–Meier curves. For this analysis, an "event" was defined as tumor volume reaching 400 mm^3 or greater. Each individual mouse was ranked as a 1 (event occurred) or a 0 (event did not occur) and the time to event (in days) was determined. When an individual was ranked as 0 (event did not occur), a time to event of 88 days (number of days in the 12.5 week study) was recorded. χ^2 and *P* values were determined by the log-rank test. All statistical analysis was conducted using GraphPad Prism software. A *P* value of <0.05 was considered significant.

Results

Expression of CD22 in lung cancer

Screening CD22-binding in various epithelial cell lines identified binding of the anti-CD22 mAb, HB22.7, to the NSCLC cell line, A549. This finding prompted us to examine CD22 expression by flow cytometry analysis in a panel of cell lines representing the major lung cancer subtypes: adenocarcinoma (A549, H1355, H1975, HC827), squamous cell (Calu-1), bronchoalveolar (H1650), epidermoid (A427), and carcinoid (H727). Using HB22.7 as a probe, flow cytometry analysis revealed varying degrees of CD22 expression on all of the cell lines except for A427 (Fig. 1A). To verify CD22 expression, mRNA was isolated from selected lung cancer cell lines and normal bronchial epithelial cells (BEC) and RT-PCR were conducted using human CD22-specific oligonucleotides (Fig. 1B). A cDNA fragment of the predicted length was amplified from Ramos (NHL), A549, H727, H1650, and a CD22-containing plasmid but not from mRNA isolated from BEC or A427 cells, consistent with the flow cytometry data. To further validate CD22 gene expression, an siRNA approach coupled with quantitative real time PCR (qRT-PCR) was used. Transfection of Raji, A549, and H727 cells with CD22 siRNA resulted in a significant reduction in CD22 mRNA expression evidenced by RT-PCR and qRT-PCR (Fig. 1E, top and bottom, respectively).

Next, anti-CD22 immunoblot analysis was conducted to see if a protein band with the expected molecular weight for human CD22 (140 kDa) could be detected in the lung cancer cell lines. A plasma membrane protein extraction kit was used to detect the expression of CD22 in either the plasma membrane or cytosol. Using the plasma membrane preparations, a band of the appropriate size was detected in the NHL cell lines, Ramos and Raji (positive control) but not in the CD22-negative cell line, Jurkat (negative control). Notably, similar bands were detected in the lanes for A549, H727, and Calu-1 but not in the lane for the flow cytometry and PCR-negative A427 cells (Fig. 1C, top). Interestingly, the band from the H1650 cell line was smaller (~55 kDa) than expected. Furthermore, PCR analysis revealed that the smaller band observed in H1650 was due to a CD22 splice variant (data not shown). Cytosolic preparations revealed the presence of full-length CD22 in the Ramos and Raji cell lines, however, cytosolic CD22 was absent in the A549, H727, and Calu-1 cell lines (Fig. 1C, bottom). H1650 exhibited a unique band of approximately 100 kDa consistent with the hypothesis that H1650 cells express a splice variant of CD22. A 100 kDa isoform of CD22 has been identified in neuronal cells and in a murine B-lymphocyte cell line (24).

To verify expression and transcript size, a Northern blot analysis was carried out with total RNA from Ramos, A549, H1650, H727, and A427 cells (Fig. 1D). This experiment validated mRNA expression in A549 and H727 cells, low level expression in H1650 and no detectable expression in A427. To determine if the CD22 sequence was the same as that found in B cells, cDNA from A549 cells was cloned and all 2,541 base pairs of CD22 were sequenced. The sequence in A549 cells was identical to the published sequence of CD22 from B cells (data not shown; ref. 25).

We hypothesized that CD22 was aberrantly expressed in these lung cancer cell lines and that this may also be true for primary lung cancer. Therefore, archived tissue blocks from 15 patients with NSCLC and normal lung tissue were obtained and immunoperoxidase staining for CD22 expression was conducted on paraffin-embedded sectioned material. Because CD22 is heavily modified posttranslationally (siaylation; refs. 8, 26), CD22 has been difficult to detect by immunohistochemistry, however, we detected CD22 staining in 3 different lung cancer tumor types (Fig. 1F). The anti-CD22 signal was often intense in part of the tumors, but weak or undetectable in the surrounding normal lung tissue. Several additional NSCLC patient specimens also stained CD22-positive by immunohistochemistry, whereas a cytoprep of normal human lung cells obtained from bronchoscopy was CD22-negative (data not shown).

CD22-mediated cytotoxicity and receptor internalization in lung cancer

Cross-linking of CD22 with ligand-blocking anti-CD22 mAbs induces cell death in B-cell NHL (15, 16), therefore, we assessed whether this was true for CD22-expressing lung cancer cells as well. Three lung cancer cell lines, as well as Ramos cells, were tested for their responsiveness to HB22.7-mediated CD22 cross-linking. After 72 hours, cytotoxic effects of HB22.7 and rituximab (anti-CD20 control mAb) were observed in Ramos cells, as previously reported. The viability of H1650 and Calu-1 was reduced by 90% and 45%, respectively, by treatment with HB22.7. There was no cytotoxic effect in A549 cells and as expected, no cytotoxicity was induced in the lung cancer cell lines treated with rituximab (Fig. 2A). A dose response was assessed in the HB22.7-sensitive cell lines; the IC_{50} for H1650 and Calu-1 was 33 and 50 μg/mL, respectively.

While anti-CD22 mAbs mediate CD22 internalization in B cells (9) and NHL (8, 26), in lung cancer, the topic of CD22 receptor internalization has never been explored. Using a validated antibody–toxin conjugate method with the degree of internalization being proportional to the degree of cytotoxicity, we showed that HB22.7 mediates more than 80% of CD22 internalization in NHL cells (data not shown) as well as 10%

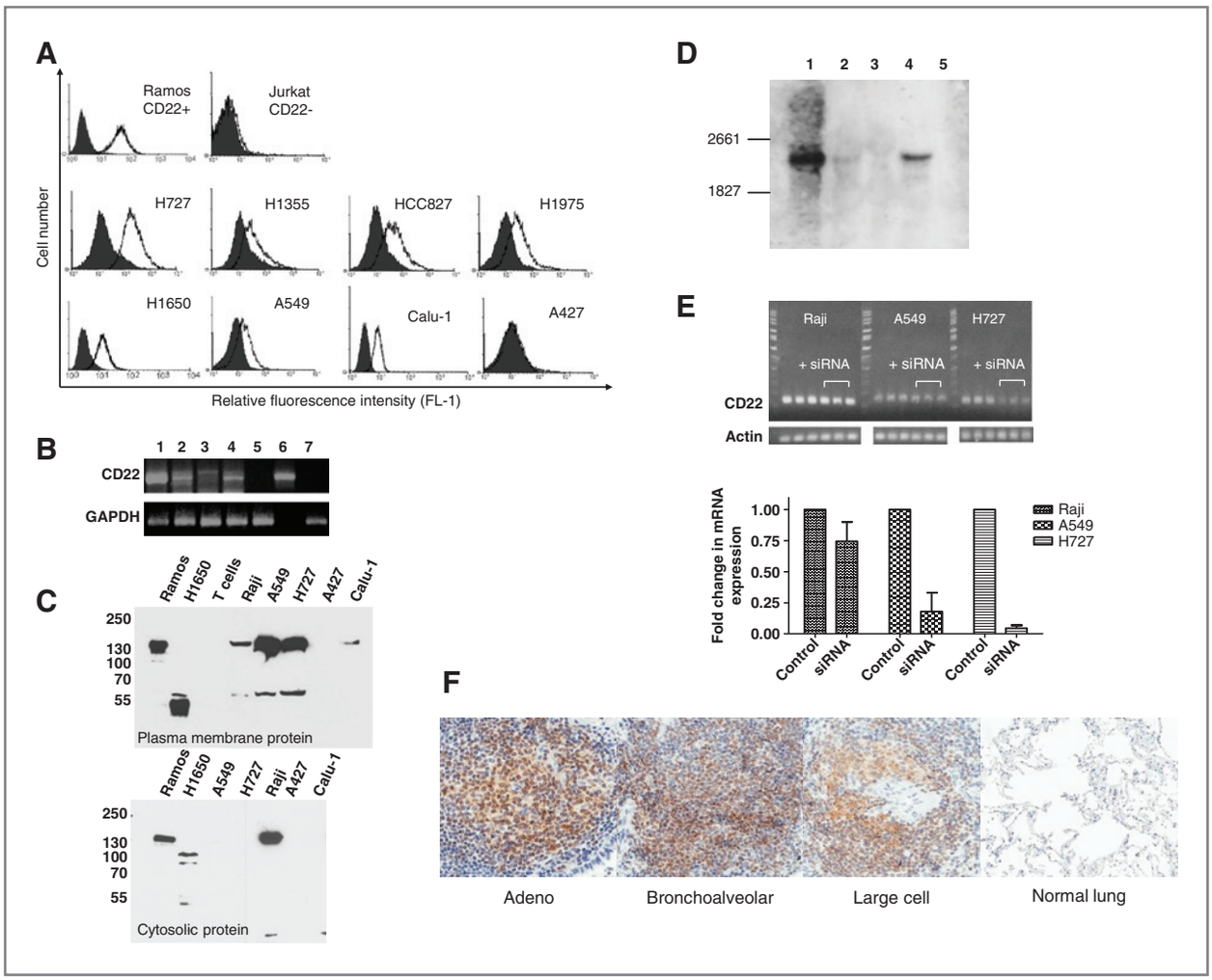

Figure 1. Expression of CD22 in lung cancer. A, various lung cancer cell lines were treated with secondary antibody (shaded) or HB22.7 plus secondary antibody (black). Ramos and Jurkat cells served as CD22-positive and negative controls, respectively. B, PCR amplification of CD22 from designated cDNA (lane 1, Ramos; lane 2, A549; lane 3, H1650; lane 4, H727; lane 5, A427; lane 6, CD22 plasmid; lane 7, BEC. C, Western blotting of CD22. The NHL cell lines, Raji and Ramos, were used as CD22-positive controls and Jurkat cells were used as a CD22-negative control. CD22 was detected from either a plasma membrane protein (top) or cytosol preparation (bottom). D, CD22 northern blot of total RNA extracted from Ramos, A549, H1650, H727, and A427 cells, lanes 1 to 5, respectively. Detection was accomplished with a DIG-dUTP–labeled DNA probe. E, RT-PCR (top) and qRT-PCR (bottom) of CD22 from designated cells treated with or without CD22 siRNA. F, immunohistochemistry of lung cancer patient biopsy specimens stained with an anti-CD22 mAb, immunoperoxidase detection, and hematoxylin and eosin counterstain (×60).

and 20% CD22-internalization in A549 and H1650 cells, respectively (Fig. 2B, top). HB22.7-mediated CD22 internalization in A549 and H1650 cells was verified using flow cytometry to detect surface-bound HB22.7 following exposure to internalizing (37°C) and noninternalizing (4°C) conditions (Fig. 2B, bottom). In both cell lines, exposure to internalizing conditions resulted in a reduction of surface-bound HB22.7 indicative of CD22 internalization mediated by the binding of HB22.7.

In primary B and NHL cells, CD22 is internalized following ligand binding (8, 26). It is unknown whether anti-CD22-mediated *in vivo* tumor suppression is mediated through host immune effector mechanisms such as ADCC, CDC, or direct cytotoxic effects. Recruitment of antibody-mediated host immune effector mechanisms can be altered by receptor internalization (27). We investigated whether humanized HB22.7 (huHB22.7) could mediate ADCC and/or CDC in A549 cells. Additional A549 cytotoxicity occurred when complement was added to huHB22.7 (2% killing by complement alone and 30% killing with complement plus huHB22.7). Little effect resulted from the addition of PBMCs to huHB22.7 above that seen with PBMCs alone (Fig. 2C).

HB22.7 effectively targets NSCLC/A549 xenografts *in vivo*

We previously showed that *in vivo* targeting of NHL xenografts could be effectively monitored with immuno-positron emission tomography (i-PET) using ^{64}Cu-DOTA-HB22.7 (22). Using the same anti-CD22 i-PET methodology, it was shown that the biodistribution and specific targeting of HB22.7 in lung cancer xenografts was similar to the biodistribution and specificity of HB22.7 in mice bearing Raji (NHL) xenografts

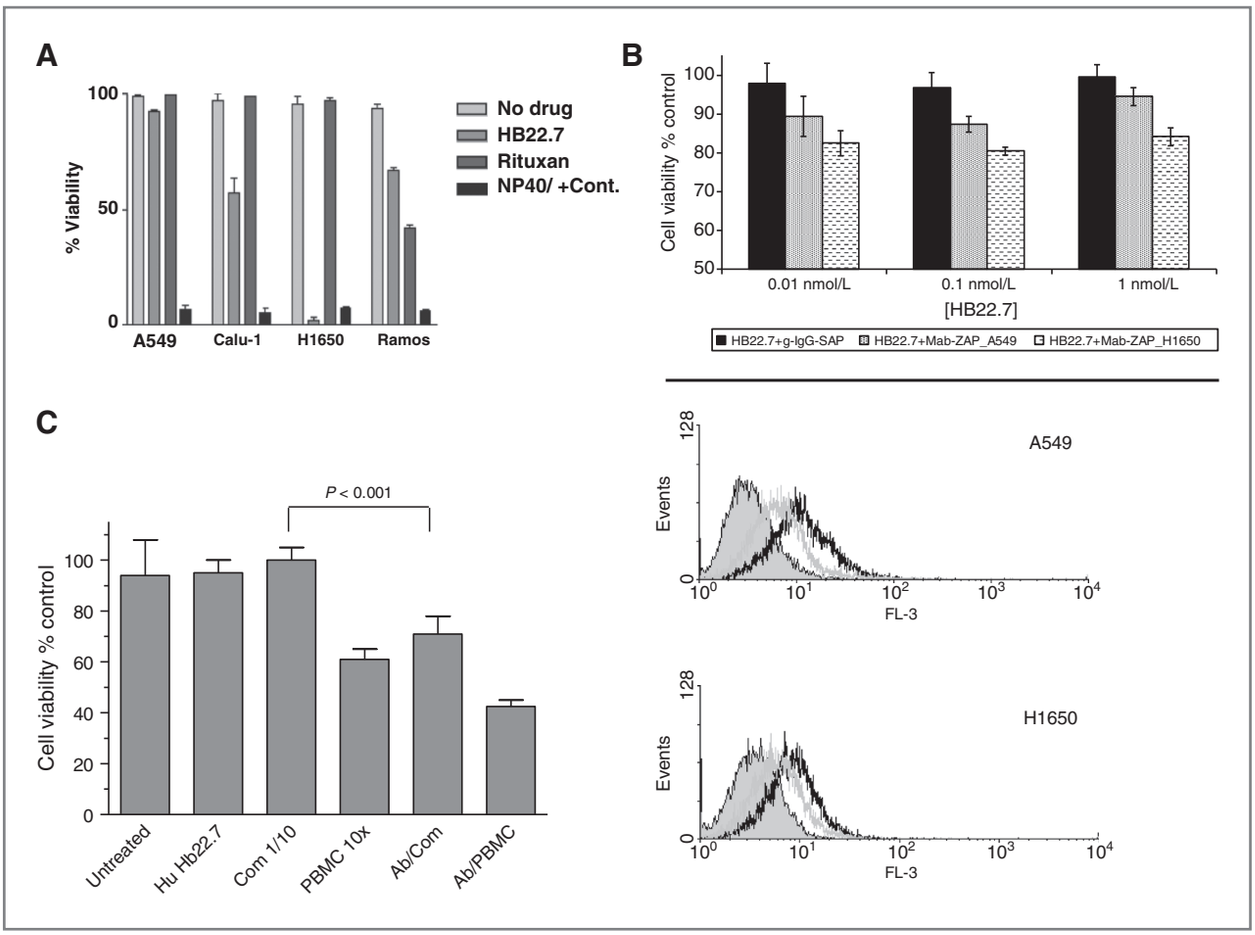

Figure 2. Anti-CD22 mAb-mediated *in vitro* cytotoxicity. A, ligation of CD22 mediates cytotoxicity of lung cancer and NHL cell lines. Cells were stimulated with HB22.7 or anti-CD20 (rituximab) at 50 μg/mL for 72 hours followed by measurement of cell viability using an MTS assay. B Internalization of CD22 was determined by assessing the cytotoxicity of an HB22.7 and anti-mouse IgG-saporin complex (top). Goat IgG-saporin was used as a nonbinding control and the 2 treatments were tested on A549 and H1650 cells. Internalization of CD22 was also assessed by measuring residual surface-bound HB22.7 following incubation at either 37°C or 4°C (bottom). Anti-mouse IgG PE-Cy5 (secondary Ab) was used to detect HB22.7. Cells were treated with secondary Ab alone (shaded), HB22.7 (4°C) + secondary Ab (black), or HB22.7 (37°C) + secondary Ab (gray). C, ADCC and CDC assays were conducted using A549 cells to determine the effect of huHB22.7 on human PBMC- or complement-mediated cytotoxicity. HuHB22.7 (50 μg/mL) was incubated with and without PBMCs (10:1 PBMC:A549) or human serum complement (1:10 dilution). A549-specific cytotoxicity was assessed and reported as a percent of the untreated control. *P* value <0.05 represents a statistically significant difference.

(Fig. 3). The majority of the radioimmunoconjugate was cleared from the blood pool by 48 hours and at this time, specific lung cancer xenograft uptake was observed; there was very little uptake in other organs including normal lung.

Activity of the anti-CD22-blocking mAb, HB22.7, against lung cancer *in vivo*

On the basis of our discovery that CD22 is expressed on lung cancer cells, and that HB22.7 bound to a majority of the lung cancer cell lines, xenograft trials were initiated to assess the preclinical efficacy of HB22.7 (Fig. 4A–D). Because H1650 cells were sensitive to the cytotoxic effects of HB22.7 *in vitro*, the ability of HB22.7 to inhibit H1650 tumor growth in nude mice was tested (Fig. 4A). HB22.7 had significant efficacy against H1650 tumors with a more than 50% reduction in tumor volume at the end of the study ($P < 0.001$). To assess the preclinical efficacy of HB22.7 in a CD22-positive, but resistant (*in vitro*) lung cancer cell line, we used an A549 xenograft model. HB22.7 significantly ($P < 0.001$) retarded the growth of established A549 tumors as compared with the untreated control (Fig. 4B). As a nonbinding control, an additional group of mice was treated with rituximab and we observed no antitumor activity. In this experiment, we also examined the effects of preemptive therapy by treating mice 24 hours after tumor cell implantation. At the end of the study period, mice that received preemptive therapy had tumor volumes that were no different than mice that received treatment of established tumors. The specificity of the HB22.7-mediated antitumor effect was shown by the lack of activity in mice bearing PC-3 (prostate cancer) xenografts (Fig. 4C).

Why HB22.7 showed *in vivo* efficacy against A549 cells that exhibited resistance to HB22.7 *in vitro* is unclear, but our data

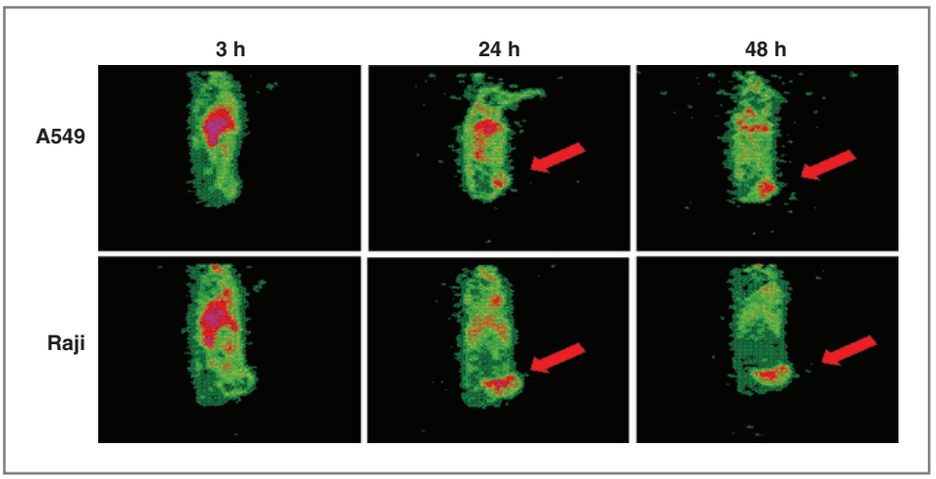

Figure 3. HB22.7 effectively targets human A549 xenografts *in vivo*. Mice bearing A549 or Raji xenografts (arrow) received ^{64}Cu-DOTA-HB22.7 (50 μCi) for I-PET using a micro-PET scanner. Top, transverse views of mice bearing A549 xenografts. Bottom, transverse views of mice bearing Raji (NHL) xenografts.

suggest that host immune effector mechanisms may be involved (Fig. 2C). The previously mentioned xenograft studies used nude mice that were irradiated to increase the likelihood of tumor establishment. Nude mice have residual natural killer (NK) cell activity capable of ADCC as well as an intact complement system. Because HB22.7 has little cytotoxic activity in A549 cells *in vitro* but shows activity in xenograft models, this residual immune function may contribute to HB22.7-mediated efficacy. An A549 xenograft model, without radiation before tumor-implantation, was conducted to assess the role of ADCC

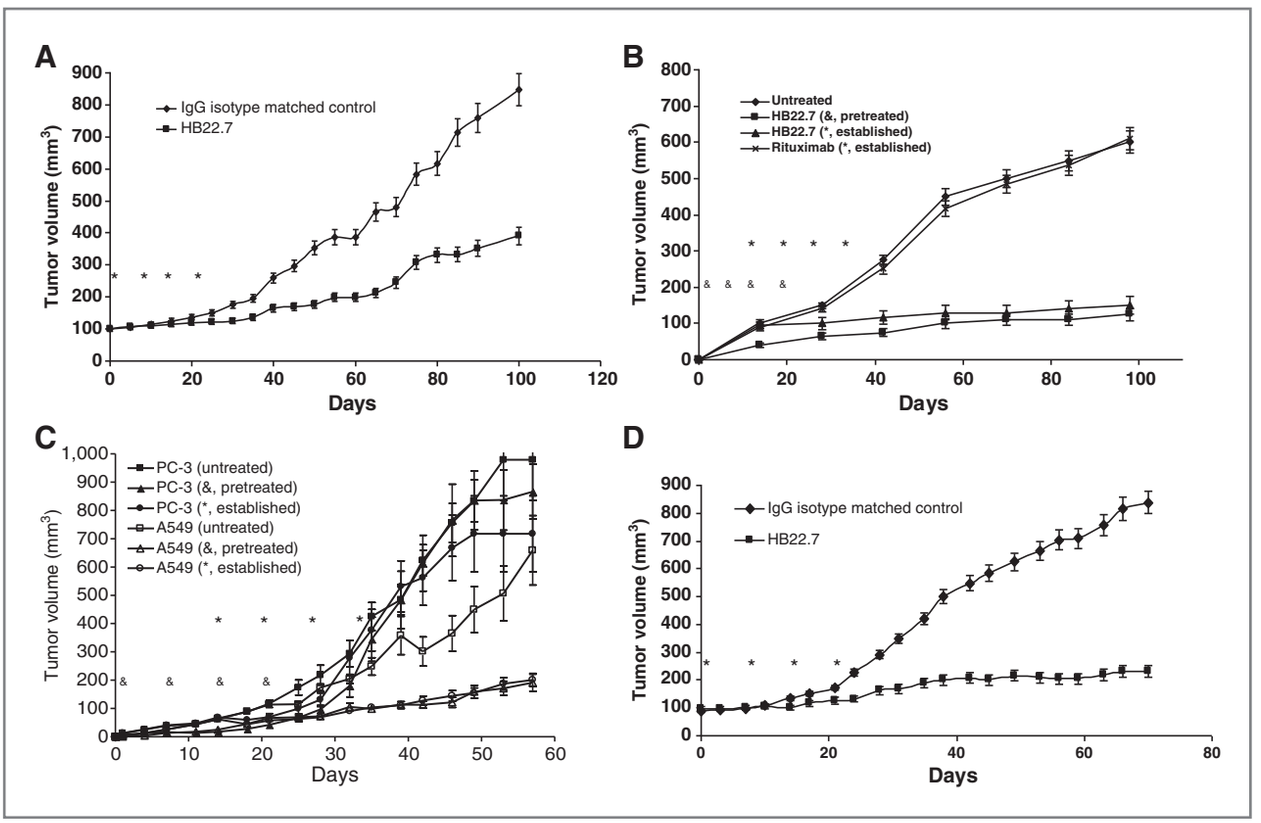

Figure 4. HB22.7 exhibits antitumor activity against lung cancer xenografts. Antibody treatment (1.4 mg) was administered weekly for 4 weeks either 24 hours after tumor cell implantation (&, pretreated) or when tumors reached a volume of approximately 100 mm^3 (*, established). A, mice bearing H1650 xenografts were intravenously injected with HB22.7 or an IgG isotype-matched control antibody. B, to assess the efficacy of HB22.7 in a CD22-positive, but resistant lung cancer cell line, mice bearing A549 xenografts were treated with HB22.7 or rituximab. C, to verify the specificity of the HB22.7-mediated antitumor effect, mice bearing A549 or PC3 (prostate cancer) xenografts were used. D, mice bearing A549 xenografts were established in nonirradiated nude mice and treated as described in A.

in HB22.7-mediated antitumor activity (Fig. 4D). In this model, HB22.7 did not exhibit increased antitumor activity in mice with normal NK cell number/activity, suggesting a limited role of ADCC. This result is consistent with our *in vitro* data, which suggests that CDC may contribute to the preclinical efficacy of HB22.7.

Efficacy of HB22.7 in a metastatic model of lung cancer

CD22 mediates B-cell homing to endothelial cells (27, 28). We hypothesized that CD22 promotes or facilitates lung cancer metastasis. To test this hypothesis, we used HB22.7 to block CD22-positive lung cancer cells from binding to CD22 ligands in a metastatic model, seeking to prevent lung metastasis after intravenous injection of lung cancer cells. Fourteen days after injecting A549 cells with or without HB22.7, mice were euthanized. Lungs were harvested and examined histologically for metastases (Fig. 5A). The differences were dramatic—most of the lung tissue from the control group of mice had a heavy tumor burden and one was nearly replaced with tumor (top right, black arrows); in HB22.7-treated mice, the lungs were virtually devoid of tumor with the exception of one micrometastasis (red arrow, bottom left). This suggests that CD22 may have a significant effect on the development of lung cancer metastasis. We also used this model to assess the effects of HB22.7 treatment on survival. Remaining mice not euthanized for histologic analysis were either continued on weekly injections of HB22.7 or IgG control. At the end of the 84-day trial, we observed a significant ($P < 0.0001$) improvement in survival with more than 90% of treated mice still alive (Fig. 5B).

Discussion

During analysis of the effects of anti-CD22 binding peptides and HB22.7 on NHL, we had an unexpected finding—HB22.7 recognized an epitope on the surface of lung cancer cells. This finding prompted us to examine CD22 expression by flow cytometry in a panel of lung cancer cell lines representing the major lung cancer subtypes. HB22.7 bound all of the cell lines except A427 and in some cases (H727) at levels nearly as high as on Ramos (NHL) cells (Fig. 1A). Evidence presented herein and elsewhere (22, 25, 29) suggest that CD22 is not expressed in normal lung epithelial cells, but CD22 expression is a common and distinct feature of malignant lung cells. Scrutiny of publicly available cDNA microarray databases (National Center for Biotechnology Information Gene Expression Omnibus) indicates that CD22 is expressed in several lung cancer cell lines that we have not tested (e.g., H1770, EBC-1, and LU65); this provides independent verification of our findings.

CD22 expression was verified using RT-PCR, Western blot and Northern blot analysis, and immunohistochemistry of patient tumor specimens (Fig. 1A–F). The pattern of CD22 expression assessed by immunohistochemistry was patchy yet distinct, with expression appearing more prominent in tightly packed clusters of tumor cells. This may be a manifestation of the adhesive properties of CD22, which, in part, forms the basis of our hypothesis that CD22 mediates lung cancer metastasis. The transcript size and sequence of CD22 found in lung cancer cells is identical to that in B cells and thus, the surface expression pattern is the only known anomaly that may

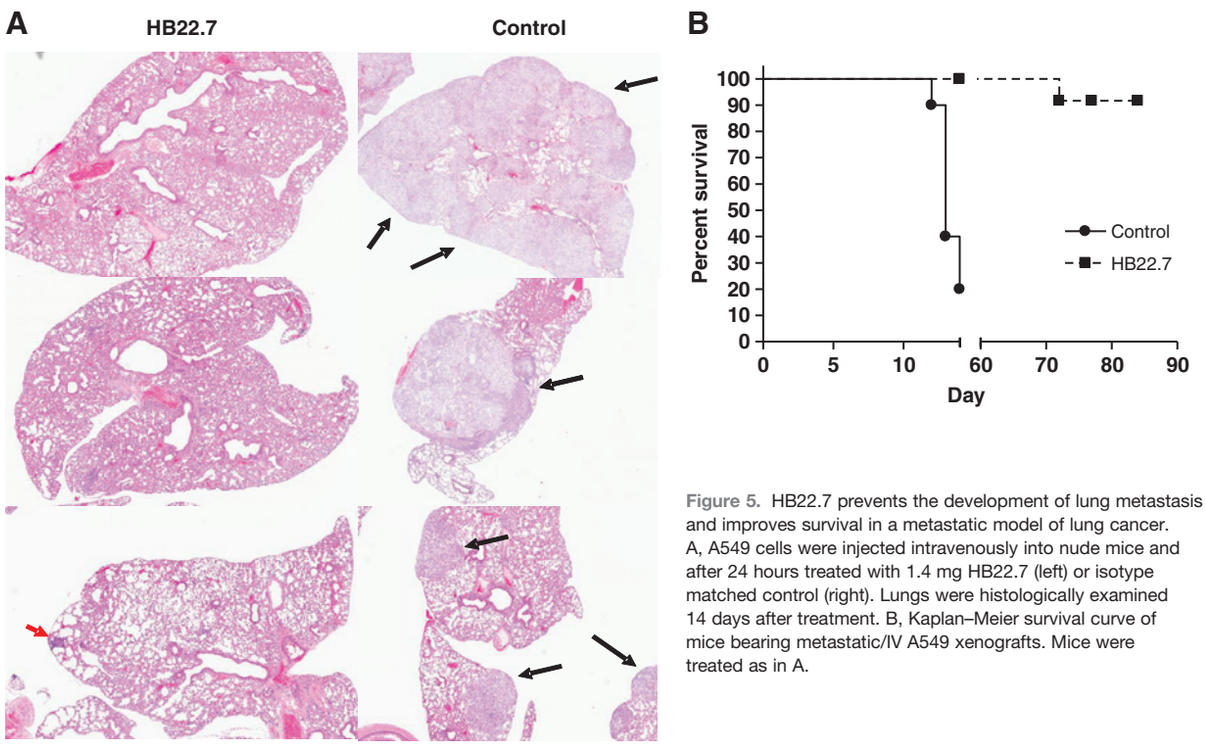

Figure 5. HB22.7 prevents the development of lung metastasis and improves survival in a metastatic model of lung cancer. A, A549 cells were injected intravenously into nude mice and after 24 hours treated with 1.4 mg HB22.7 (left) or isotype matched control (right). Lungs were histologically examined 14 days after treatment. B, Kaplan–Meier survival curve of mice bearing metastatic/IV A549 xenografts. Mice were treated as in A.

mediate a selective advantage in terms of metastasis and possibly growth. The specific role of CD22 in B cells remains controversial, but most agree that it mediates adhesion and modulates receptor-mediated signals (11, 12, 27, 28). There is also evidence that the CD22 ligand–binding domain mediates a specific survival signal in normal and malignant B cells (10). We previously showed that the CD22 ligand-blocking mAb, HB22.7, has significant lymphomacidal properties. While the mechanism of HB22.7-mediated lymphomacidal activity remains poorly understood, previous studies using murine models have suggested that the effects of HB22.7 are specifically mediated by inhibiting the effects of CD22 ligand binding (10). We also showed selective killing of lung cancer cells *in vitro* and *in vivo* (Figs. 2A and Fig. 4A–D).

While the growth of both H1650 and A549 tumor xenografts were inhibited by HB22.7, only H1650 had *in vitro* cytotoxicity; therefore, we examined the possibility that host immune effector mechanisms contribute to the cytotoxic effects (Fig. 2C). ADCC and CDC assays showed that complement may contribute to the *in vivo* activity (the complement system is intact in nude mice). It remains unknown why HB22.7 showed preclinical efficacy in A549 xenografts but not *in vitro*; however, this phenomenon might be explained by the observation that HB22.7 mediates a survival signal by blocking ligand binding in the context of cellular interactions. Thus, *in vivo* HB22.7-mediated killing may, in part, be secondary to the CD22 ligand blocking properties not completely dependent on direct CD22-mediated effects. Previous studies with mAbs that bind internalizing receptors have suggested that host immune effector mechanism may have a lesser role. While CD22 on A549 and H1650 lung cancer cells did show some internalization, it was approximately 50% less than what was observed on Ramos cells (Fig. 2B). CD22 has been shown to mediate both homotypic and heterotypic adhesion with known CD22 ligand-bearing cells that include nearly all hematopoietic cell types as well as endothelial cells (8, 9, 25). The aberrant expression of CD22 on lung cancer cells as well as its role in B-cell homing is the basis for our hypothesis that CD22 in lung cancer cells may be involved in the process of lung cancer metastasis. To test this, we used an intravenous, metastatic model of lung cancer (23). Treatment with HB22.7 resulted in an enormous reduction in the number and size of tumor implants in the lungs. There were virtually no tumors detected in the lungs of mice treated with HB22.7 (Fig. 5A). This model also allowed us to study the effects of treatment with HB22.7 on survival. While some mice were euthanized for histologic examination, those that were observed had a significant improvement in overall survival when treated with HB22.7; 100% of untreated mice died by day 40 but more than 90% of the treated survived the entire study period (Fig. 5B).

In summary, the identification of CD22 on lung cancer is a milestone for future development of lung cancer–specific therapeutics. In addition, examination of the role of CD22 may ultimately result in a better understanding of the pathogenesis and invasiveness of lung cancer.

Disclosure of Potential Conflicts of Interest

No potential conflicts of interest were disclosed.

Authors' Contributions

Conception and design: J.M. Tuscano, R.T. O' Donnell
Development of methodology: J.M. Tuscano, R.T. O' Donnell
Acquisition of data (provided animals, acquired and managed patients, provided facilities, etc.): J.M. Tuscano, J. Kato, D. Pearson, C. Xiong, L.F. Newell, R.T. O' Donnell
Analysis and interpretation of data (e.g., statistical analysis, biostatistics, computational analysis): J.M. Tuscano, J. Kato, R.T. O' Donnell
Writing, review, and/or revision of the manuscript: J.M. Tuscano, J. Kato, Y. P. Ma, D.R. Gandara, R.T. O' Donnell
Administrative, technical, or material support (i.e., reporting or organizing data, constructing databases): R.T. O' Donnell
Study supervision: J.M. Tuscano, R.T. O' Donnell

Acknowledgments

This work was supported by the Schwedler Family Foundation and the deLeuze Non-toxic Cure for Lymphoma Fund.

The costs of publication of this article were defrayed in part by the payment of page charges. This article must therefore be hereby marked *advertisement* in accordance with 18 U.S.C. Section 1734 solely to indicate this fact.

Received January 23, 2012; revised August 13, 2012; accepted August 31, 2012; published OnlineFirst September 17, 2012.

References

1. JD M. Neoplasms of the Lung;2005.
2. Detterbeck FC, Boffa DJ, Tanoue LT. The new lung cancer staging system. Chest 2009;136:260–71.
3. Wang T, Nelson RA, Bogardus A, Grannis FW Jr. Five-year lung cancer survival: which advanced stage nonsmall cell lung cancer patients attain long-term survival? Cancer 2010;116:1518–25.
4. Katzel JA, Fanucchi MP, Li Z. Recent advances of novel targeted therapy in non-small cell lung cancer. J Hematol Oncol 2009;2:2.
5. Stinchcombe TE, Socinski MA. Current treatments for advanced stage non-small cell lung cancer. Proc Am Thoracic Soc 2009;6: 233–41.
6. Sun S, Schiller JH, Spinola M, Minna JD. New molecularly targeted therapies for lung cancer. J Clin Invest 2007;117:2740–50.
7. Collins BE, Blixt O, Han S, Duong B, Li H, Nathan JK, et al. High-affinity ligand probes of CD22 overcome the threshold set by cis ligands to allow for binding, endocytosis, and killing of B cells. J Immunol 2006;177:2994–3003.
8. Crocker PR, Paulson JC, Varki A. Siglecs and their roles in the immune system. Nat Rev Immunol 2007;7:255–66.
9. Engel P, Wagner N, Miller AS, Tedder TF. Identification of the ligand-binding domains of CD22, a member of the immunoglobulin superfamily that uniquely binds a sialic acid-dependent ligand. J Exp Med 1995;181:1581–6.
10. Haas KM, Sen S, Sanford IG, Miller AS, Poe JC, Tedder TF. CD22 ligand binding regulates normal and malignant B lymphocyte survival in vivo. J Immunol 2006;177:3063–73.
11. Tedder TF, Poe JC, Haas KM. CD22: a multifunctional receptor that regulates B lymphocyte survival and signal transduction. Adv Immunol 2005;88:1–50.
12. Tedder TF, Tuscano J, Sato S, Kehrl JH. CD22, a B lymphocyte-specific adhesion molecule that regulates antigen receptor signaling. Annu Rev Immunol 1997;15:481–504.
13. Tuscano J, Engel P, Tedder TF, Kehrl JH. Engagement of the adhesion receptor CD22 triggers a potent stimulatory signal for B cells and blocking CD22/CD22L interactions impairs T-cell proliferation. Blood 1996;87:4723–30.
14. Tuscano JM, Engel P, Tedder TF, Agarwal A, Kehrl JH. Involvement of p72syk kinase, p53/56lyn kinase and phosphatidyl inositol-3 kinase in

signal transduction via the human B lymphocyte antigen CD22. Eur J Immunol 1996;26:1246–52.
15. Tuscano JM, Riva A, Toscano SN, Tedder TF, Kehrl JH. CD22 cross-linking generates B-cell antigen receptor-independent signals that activate the JNK/SAPK signaling cascade. Blood 1999;94:1382–92.
16. Tuscano JM, O'Donnell RT, Miers LA, Kroger LA, Kukis DL, Lamborn KR, et al. Anti-CD22 ligand-blocking antibody HB22.7 has independent lymphomacidal properties and augments the efficacy of 90Y-DOTA-peptide-Lym-1 in lymphoma xenografts. Blood 2003;101:3641–7.
17. Hatakeyama S, Yamamoto H, Ohyama C. Tumor formation assays. Methods Enzymol 2010;479:397–411.
18. Joehanes R, Nelson JC. QGene 4.0, an extensible Java QTL-analysis platform. Bioinformatics 2008;24:2788–9.
19. Simon P. Q-Gene: processing quantitative real-time RT-PCR data. Bioinformatics 2003;19:1439–40.
20. Kohls MD, Lappi DA. Mab-ZAP: a tool for evaluating antibody efficacy for use in an immunotoxin. BioTechniques 2000;28:162–5.
21. Gerber HP, Kung-Sutherland M, Stone I, Morris-Tilden C, Miyamoto J, McCormick R, et al. Potent antitumor activity of the anti-CD19 auristatin antibody drug conjugate hBU12-vcMMAE against rituximab-sensitive and -resistant lymphomas. Blood 2009;113:4352–61.
22. Martin SM, O'Donnell RT, Kukis DL, Abbey CK, McKnight H, Sutcliffe JL, et al. Imaging and pharmacokinetics of (64)Cu-DOTA-HB22.7 administered by intravenous, intraperitoneal, or subcutaneous injection to mice bearing non-Hodgkin's lymphoma xenografts. Mol Imaging Biol 2009;11:79–87.
23. Guilbaud N, Kraus-Berthier L, Saint-Dizier D, Rouillon MH, Jan M, Burbridge M, et al. Antitumor activity of S 16020–2 in two orthotopic models of lung cancer. Anticancer drugs 1997;8:276–82.
24. Mott RT, Ait-Ghezala G, Town T, Mori T, Vendrame M, Zeng J, et al. Neuronal expression of CD22: novel mechanism for inhibiting microglial proinflammatory cytokine production. Glia 2004;46:369–79.
25. Wilson GL, Fox CH, Fauci AS, Kehrl JH. cDNA cloning of the B cell membrane protein CD22: a mediator of B-B cell interactions. J Exp Med 1991;173:137–46.
26. Shan D, Press OW. Constitutive endocytosis and degradation of CD22 by human B cells. J Immunol 1995;154:4466–75.
27. Nitschke L, Floyd H, Ferguson DJ, Crocker PR. Identification of CD22 ligands on bone marrow sinusoidal endothelium implicated in CD22-dependent homing of recirculating B cells. J Exp Med 1999;189:1513–8.
28. Hanasaki K, Varki A, Powell LD. CD22-mediated cell adhesion to cytokine-activated human endothelial cells. Positive and negative regulation by alpha 2–6-sialylation of cellular glycoproteins. J Biol Chem 1995;270:7533–42.
29. Postema EJ, Raemaekers JM, Oyen WJ, Boerman OC, Mandigers CM, Goldenberg DM, et al. Final results of a phase I radioimmunotherapy trial using (186)Re-epratuzumab for the treatment of patients with non-Hodgkin's lymphoma. Clin Cancer Res 2003;9:3995S-4002S.